Chapter 5

Femtosecond Laser Pulses

Most of the experiments described in this work were performed using femtosecond laser pulses delivered from a commercial multipass amplification laser system [Ste03]. Generally, the name "femtosecond laser pulses" is related to laser pulses with a duration on the femtosecond ($1\,\text{fs} = 1 \times 10^{-15}\,\text{s}$) time scale. But in this work the term "femtosecond laser pulse" is used for a pulse with a duration around 30 fs. Shorter pulses with a duration below 10 fs are called "sub-10 fs pulses".

This chapter starts with a mathematical representation of an electromagnetic field needed for the description of laser pulses. Then, the laser system together with methods and techniques of femtosecond and sub-10 fs laser pulses generation as well as additional equipment employed in the experiments for the operation and manipulation of laser pulses are described. This description is essentially based on Refs. [Rul05, DRu06, HSc08]. After that, the "classical" intensity averaging theory for elliptically polarised light [SRS09] is given. Finally, the pulse shaping technique is presented.

5.1 Mathematical Description of Laser Pulses

In the general case, the electric field strength of an electromagnetic wave is a function of spatial coordinates and time. Often, such functional dependence can be factorised and the electric field can be represented as a product of two functions depending on spatial coordinates and time, respectively. For any given point in space the strength of the electric field is only a function of time. It is convenient to write the real electric field $E(t)$ of linear polarised light

(e.g. $\mathbf{E} \parallel x$) as

$$E(t) = \frac{1}{2}\left(E^{+}(t) + E^{-}(t)\right) \quad , \tag{5.1}$$

where $E^{+}(t)$ and $E^{-}(t)$ are the complex electric field and its complex conjugate. The complex electric field can be presented by a product of an amplitude function $A(t)$ and a phase term

$$E^{+}(t) = A(t)e^{-i[\omega_0 t - \phi(t)]} \tag{5.2}$$

and

$$E^{-}(t) = A(t)e^{i[\omega_0 t - \phi(t)]} \quad , \tag{5.3}$$

where ω_0 is a carrier or central frequency, and $\phi(t)$ is a temporal phase. In quantum mechanics the $E^{+}(t)$ field is responsible for absorption, the $E^{-}(t)$ field for emission. The intensity of a pulse $I(t)$ is related with the pulse amplitude as

$$I(t) = \varepsilon_0 c A^2(t)\cos^2\left(\omega_0 t - \phi(t)\right) \quad , \tag{5.4}$$

where ε_0 is the dielectric constant in vacuum and c is the speed of light. If $A(t)$ varies slowly, the period averaged intensity is

$$\langle I(t)\rangle = \frac{\varepsilon_0 c}{2}A^2(t) \quad . \tag{5.5}$$

The temporal amplitude and the phase contain all information about the laser pulse. The complex electric field can be expressed by inverse Fourier integrals

$$E^{+}(t) = \frac{1}{2\pi}\int_{-\infty}^{\infty}\tilde{E}^{+}(\omega)e^{i\omega t}\,d\omega \tag{5.6}$$

and

$$E^{-}(t) = \frac{1}{2\pi}\int_{-\infty}^{\infty}\tilde{E}^{-}(\omega)e^{i\omega t}\,d\omega \quad , \tag{5.7}$$

where $\tilde{E}^{+}(\omega)$ and $\tilde{E}^{+}(\omega)$ are a complex representation of the electric field in a frequency domain (spectral representation) and its complex conjugate. By analogy, the complex electric field in a frequency domain

$$\tilde{E}(\omega) = \frac{1}{2}\left(\tilde{E}^{+}(\omega) + \tilde{E}^{-}(\omega)\right) \tag{5.8}$$

can be presented by a product of an spectral amplitude $\tilde{A}(\omega)$ and a phase term

$$\tilde{E}^{+}(\omega) = \tilde{A}(\omega)e^{i\varphi(\omega)} \tag{5.9}$$

and

$$\tilde{E}^{-}(\omega) = \tilde{A}(\omega)e^{-i\varphi(\omega)} \quad , \tag{5.10}$$

where $\varphi(\omega)$ is a spectral phase. The spectral representation is related to the temporal representation by the Fourier transformation

$$\tilde{E}^{+}(\omega) = \int_{-\infty}^{\infty} E^{+}(t)e^{-i\omega t}\,dt \tag{5.11}$$

and

$$\tilde{E}^{-}(\omega) = \int_{-\infty}^{\infty} E^{-}(t)e^{-i\omega t}\,dt \quad . \tag{5.12}$$

The period averaged spectral intensity (spectrum) of a pulse $\tilde{I}(\omega)$ is related to the spectral amplitude as

$$\tilde{I}(\omega) = \frac{\varepsilon_0 c}{4\pi}\tilde{A}^2(\omega) \quad . \tag{5.13}$$

Both representations either in the time domain using a temporal amplitude and a phase or in the frequency domain using a spectral amplitude and a phase are equivalent.

The mathematical description of the temporal amplitude and intensity as well as the spectral amplitude and intensity distribution for some commonly used pulse shapes are summarised in Table 5.1. These pulse shapes are standard for the analytical calculations and they are often used to approximate experimental data. A rectangular pulse does not have wings, therefore it is a very poor approximation of reality but most simple for calculations. A Gaussian pulse is also quite simple for calculations. It has quickly falling wings ($\propto e^{-t^2}$) which is not always true in a real experiment. The sech^2 pulse has wings which are slowly falling ($\propto e^{-t}$). This pulse shape is often more appropriate to describe experimental situations precisely. And finally, Lorentzian pulses with very large wings ($\propto \frac{1}{t}$) may also be useful sometimes.

Usually, pulse durations τ are given as full width at half maximum intensity (FWHM) as done so in Table 5.1. Sometimes the pulse duration is determined at the intensity levels $1/e$ ($\tau_{1/e}$) or $1/e^2$ (τ_{1/e^2}). For a rectangular pulse durations determined at the different intensity levels are identical. For Gaussian, sech^2, and Lorentzian pulses these durations are related as follows

$$\text{Gaussian: } \tau = \sqrt{\ln 2}\tau_{1/e} = \sqrt{\frac{\ln 2}{2}}\tau_{1/e^2} \quad , \tag{5.14}$$

$$\text{sech}^2\text{: } \tau = 0.812\tau_{1/e} = 0.532\tau_{1/e^2} \quad , \tag{5.15}$$

and

$$\text{Lorentzian: } \tau = 0.763\tau_{1/e} = 0.396\tau_{1/e^2} \quad . \tag{5.16}$$

Table 5.1: The mathematical description (taken from [DRu06]) of some pulse shapes in the time and frequency domains. τ and ω_0 are temporal FWHM and carrier frequency, respectively. Frequency amplitudes and intensities are given without normalisation factors.

Shape	Temporal amplitude	Temporal intensity
Rectangular	1 for $\left\|\frac{t}{\tau}\right\| \leq \frac{1}{2}$, 0 else	1 for $\left\|\frac{t}{\tau}\right\| \leq \frac{1}{2}$, 0 else
Gaussian	$\exp\left[-2\ln 2\left(\frac{t}{\tau}\right)^2\right]$	$\exp\left[-4\ln 2\left(\frac{t}{\tau}\right)^2\right]$
sech^2	$\mathrm{sech}\left[2\ln\left(1+\sqrt{2}\right)\frac{t}{\tau}\right]$	$\mathrm{sech}^2\left[2\ln\left(1+\sqrt{2}\right)\frac{t}{\tau}\right]$
Lorentzian	$\left[1+\frac{4}{1+\sqrt{2}}\left(\frac{t}{\tau}\right)^2\right]^{-1}$	$\left[1+\frac{4}{1+\sqrt{2}}\left(\frac{t}{\tau}\right)^2\right]^{-2}$
Shape	**Frequency amplitude**	**Frequency intensity**
Rectangular	$\tau\,\mathrm{sinc}\left[\frac{\tau(\omega-\omega_0)}{2}\right]$	$\tau^2\,\mathrm{sinc}^2\left[\frac{\tau(\omega-\omega_0)}{2}\right]$
Gaussian	$\sqrt{\frac{\pi}{2\ln 2}}\tau\exp\left[-\frac{\tau^2(\omega-\omega_0)^2}{8\ln 2}\right]$	$\frac{\pi}{2\ln 2}\tau^2\exp\left[-\frac{\tau^2(\omega-\omega_0)^2}{4\ln 2}\right]$
sech^2	$\frac{\pi}{2\ln(1+\sqrt{2})}\tau\,\mathrm{sech}\left[\frac{\pi\tau(\omega-\omega_0)}{4\ln\left(1+\sqrt{2}\right)}\right]$	$\left(\frac{\pi}{2\ln(1+\sqrt{2})}\right)^2\tau^2\,\mathrm{sech}^2\left[\frac{\pi\tau(\omega-\omega_0)}{4\ln\left(1+\sqrt{2}\right)}\right]$
Lorentzian	$\frac{\pi\sqrt{1+\sqrt{2}}}{2}\tau\exp\left[-\frac{\sqrt{1+\sqrt{2}}\tau\lvert\omega-\omega_0\rvert}{2}\right]$	$\frac{\pi^2(1+\sqrt{2})}{4}\tau^2\exp\left[-\sqrt{1+\sqrt{2}}\tau\lvert\omega-\omega_0\rvert\right]$

The intensity autocorrelation function

$$S(\delta) = \int_{-\infty}^{\infty} I(t)I(t-\delta)\,dt \tag{5.17}$$

plays an important role in temporal pulse characterisation techniques. It is determined as the time integral of temporal pulse intensity function $I(t)$ multiplied by its shifted replica $I(t-\delta)$. Here the pulse replica is used as a gate to scan the same pulse. The autocorrelation function is always symmetric and centred around $\delta = 0$. The width of the autocorrelation function τ_{AC} is determined by the pulse width τ:

$$\tau_{AC} = \frac{1}{D_{AC}}\tau \quad , \tag{5.18}$$

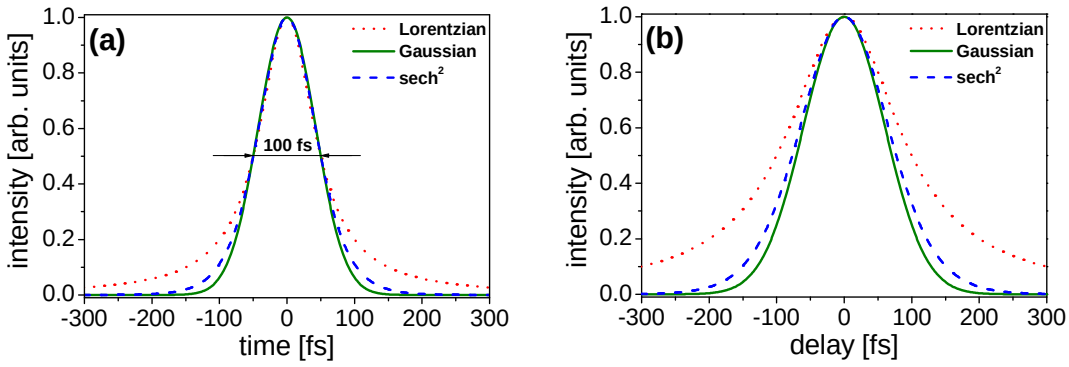

Figure 5.1: (a) Pulses of different shapes, (Lorentzian, Gaussian, and sech^2 with 100 fs FWHM) and (b) their calculated autocorrelation functions.

where D_{AC} is the deconvolution factor depending on the pulse shape. The values of these factors for different commonly used pulse shapes are summarised in Table 5.2. Calculated intensity autocorrelation traces for the pulses with different shapes but with constant width of 100 fs FWHM are plotted in Fig. 5.1. While all three pulses have the same FWHM, the width of the autocorrelation traces differs according to the values of D_{AC} from the Table 5.2.

If a spectral phase $\varphi(\omega)$ varies slowly with the frequency ω, it can be expanded into the Taylor series around the carrier frequency ω_0

$$\varphi(\omega) = \sum_{k=0}^{\infty} \frac{\varphi^{(k)}(\omega_0)}{k!}(\omega - \omega_0)^k \tag{5.19}$$

with

$$\varphi^{(k)}(\omega_0) = \left.\frac{\partial^k \varphi(\omega)}{\partial \omega^k}\right|_{\omega=\omega_0} . \tag{5.20}$$

The first term $\varphi(\omega_0)$ in Eq. (5.19) describes the absolute phase of the pulse in the time domain. The first derivative $\varphi'(\omega_0) = T_g(\omega_0)$ is the so-called "group delay" (GD). GD leads to a shift of the pulse envelope in the time domain. The second derivative $\varphi''(\omega_0) = D_2(\omega_0)$ is the "group delay dispersion" (GDD) (also sometimes called "second order dispersion") . $\varphi'''(\omega_0) = D_3(\omega_0)$ and $\varphi''''(\omega_0) = D_4(\omega_0)$ are the "third (TOD) and fourth (FOD) order dispersion", respectively. Since these higher order derivatives (GDD and higher) describe the frequency dependence of the GD

$$D_2(\omega_0) = \varphi''(\omega_0) = \left.\frac{\partial T_g(\omega)}{\partial \omega}\right|_{\omega=\omega_0} , \tag{5.21}$$

$$D_3(\omega_0) = \varphi'''(\omega_0) = \left.\frac{\partial^2 T_g(\omega)}{\partial \omega^2}\right|_{\omega=\omega_0} \quad , \tag{5.22}$$

and

$$D_4(\omega_0) = \varphi''''(\omega_0) = \left.\frac{\partial^3 T_g(\omega)}{\partial \omega^3}\right|_{\omega=\omega_0} \quad , \tag{5.23}$$

they are responsible for dispersive effects and changes in temporal structure of the pulse envelope.

By analogy, the temporal phase $\phi(t)$ can be expanded into the Taylor series around time zero for small derivations

$$\phi(t) = \sum_{k=0}^{\infty} \frac{\phi^{(k)}(0)}{k!} t^k \tag{5.24}$$

with

$$\phi^{(k)}(0) = \left.\frac{\partial^k \phi(t)}{\partial t^k}\right|_{t=0} \quad . \tag{5.25}$$

The time derivative of the temporal phase defines the instantaneous frequency $\omega(t)$

$$\omega(t) = \omega_0 - \frac{d\phi(t)}{dt} \quad . \tag{5.26}$$

The first term in the Taylor series (Eq. (5.24)) $\phi(0)$ is the absolute phase of the pulse. The absolute phase gives the temporal relation of the pulse envelope with respect to the underlying carrier oscillation. The first derivative $\phi'(0)$ in the second term, which is linear with time, describes a shift of the carrier frequency ω_0. The term with $\phi''(0)$ corresponds to the linear motion of the instantaneous frequency. Such term is named a linear chirp. The frequency rising (decreasing) with time is referred to as up-chirp (down-chirp). The next terms are the quadratic, cubic, and so on chirp.

If the instantaneous frequency for a pulse does not depend on time $(\omega(t) = const)$, such pulse is called a "bandwidth limited" or "Fourier transform limited" pulse. In this case the pulse duration τ is determined by its spectral width only

$$\tau \Delta\omega = 2\pi K_{TB} \quad , \tag{5.27}$$

where τ and $\Delta\omega$ are FWHM of intensity profile in the time and frequency domains respectively. K_{TB} is a constant which depends on a pulse shape. The values of K_{TB} for some commonly used pulse shapes are given in Table 5.2. Usually, Eq. (5.27) is known as a "time-bandwidth product". It indicates that for the achievement of the shorter pulse duration one needs to apply a greater frequency bandwidth. Because real laser pulses are mostly not bandwidth limited, Eq. (5.27) provides only the lower limit for estimations of the pulse duration.

Table 5.2: Deconvolution factors D_{AC} and time-bandwidth products K_{TB} for the various shapes of laser pulses.

Pulse shape	D_{AC}	K_{TB}
Rectangular	1.0000	0.443
Gaussian	$1/\sqrt{2}$	0.441
sech^2	0.6482	0.315
Lorentzian	0.5000	0.142

5.2 Generation of Femtosecond Laser Pulses

5.2.1 Femtosecond Oscillators

The standard approach to produce femtosecond laser pulses includes pulse generation by a mode-locked oscillator followed by chirped pulse amplification (CPA), in which an initial laser pulse is stretched by a prism or grating stretcher, then amplified in regenerative or multipass schemes, and finally recompressed [SMo85, ZHM95, BDM98].

Generally, the construction of a femtosecond oscillator is rather straight forward and consists of the same elements as any laser: a resonator cavity with (partially) reflecting end mirrors and a gain medium inside [SSK94, CSM96]. The key difference in comparison with lasers or long pulsed lasers is (aside from a medium with broad band amplification) the presence of a dispersive element (a pair of prisms or chirped mirrors) in the cavity to control the spectral dispersion. This element allows one to compensate the dispersion introduced by the gain medium and other optical parts. Typically, an oscillator is pumped by a continuous wave (cw) laser. The pumping beam is focused into the active medium collinear with the mode of the cavity itself.

For a given wavelength λ a discrete number of longitudinal modes can exist inside the oscillator cavity for which

$$L = n\frac{\lambda}{2} \quad , \tag{5.28}$$

where L is the cavity length and n an integer describing one longitudinal mode. At the same

time, only such longitudinal modes for which the gain of the pumped medium exceeds the laser threshold on the gain curve of the pumped laser medium can oscillate in the cavity. The output radiation field consists of the sum over all fields in the oscillating modes. If there is no constant phase relation between the modes, the intensity of the output radiation fluctuates randomly as a function of time without any regular temporal structure. The so-called "mode locking" holds all longitudinal modes in phase and constructive interference between the phase locked modes generates a single pulse circulating in the cavity. Each reflection of this pulse from a partly transmitting cavity mirror produces a pulse leaving the cavity. It forms the output laser radiation composed of a laser pulses train. The separation between the pulses in the train is equal to the round trip time T_{RT} of the cavity

$$T_{RT} = \frac{2L}{c} \quad , \tag{5.29}$$

where c is a speed of light.

All techniques of mode locking can be divided into two groups: active and passive mode locking [HBe87]. Active mode locking involves either a periodic modulation of the cavity losses with the period corresponding to the cavity round trip time or a periodic round trip phase change. It can be achieved by an acousto-optical modulator (AOM) or an electro-optical modulator (EOM) placed inside the cavity [KSi70]. The first device is used to introduce a periodic modulation of the cavity loses, while the second one produces a time dependent phase variation. Active mode locking has two main disadvantages. First, the modulating frequency of AOM or EOM has to match the reciprocal of the cavity round trip time. Even very small cavity length drifts can lead to frequency mismatching and a strong timing jitter or even to chaotic behaviour. This problem can be solved using the so-called "regenerative mode locking technique" [SES91]. This technique uses a feedback circuit for automatic adjustment of the modulating frequency to keep the synchronisation intact. Second, the pulse compression mechanism introduced by active mode locking itself is quite weak. An active modulator initiates a strong compression as long as the duration of the compressed pulse is larger than the modulating function. But when the pulse duration reaches the width of the modulating function further compression becomes very weak. Hence, active mode locking can be used to produce laser pulses with a duration on the picosecond time scale. Shorter pulse durations can be achieved by application of active mode locking driven at high harmonics of the round trip frequency (harmonic mode locking) [JLK98] or with passive mode locking.

In passive mode locking a fixed phase relationship is created by a saturable absorber, often thin semiconductor films or organic dyes. Their absorption coefficient decreases with increasing intensity of the light passing through. Because the transmission of the absorber follows the incoming intensity, a pulse propagating through the saturable absorber undergoes weak interaction with the absorber around its peak intensity, while the less intensive wings are exposed to larger losses. Therefore, the pulse is shortened during each propagation through the saturable absorber till the pulse duration reaches the absorption recovery time [Pen86]. This is a regime of a fast saturable absorber, where the losses induced by the absorber follow the pulse intensity profile. If the pulse duration is shorter than the absorption recovery time, the saturable absorber is slow. In the slow regime the induced losses do not follow the pulse intensity profile. The slow saturable absorbers can be utilised for the generation of femtosecond pulses combining this method with the saturable amplification [GSS90] or in colliding pulse mode locking [FGS81].

The most important type of passive mode locking, especially for the generation of femtosecond pulses, is the so-called "Kerr lens mode locking" (KLM) [BSC92]. The name KLM comes from the Kerr type nonlinearity, in which the refractive index n of a medium is altered by the applied optical intensity I according to

$$n = n_0 + n_2 I \quad , \tag{5.30}$$

where n_0 is the normal and n_2 the nonlinear refractive index. n_2 has a very small value, and therefore the nonlinearity of the refractive index is negligible under normal conditions. But inside a laser cavity it is possible to reach intensities at which nonlinear effects start to play a significant role. A pulse propagating through the Kerr active medium experiences the highest refractive index for the central and most intense part. It thus produces an intensity sensitive phase modulation. It also leads to self-focusing and creation of a "Kerr lens". This effect can be used to induce instantaneous intensity dependent losses inside the cavity. They can be weak for a short intensive pulse, while less intensive pulses or cw radiation are exposed to larger losses. The action of the Kerr type nonlinearity is analogue to very fast saturable absorbers providing a modulation function which can follow even femtosecond pulse profiles. This type of mode locking is successfully used for the generation of laser pulses with a duration down to $10\,\mathrm{fs}$ [CMK94, ZTH94]. Its main disadvantage is a poor long-term stability of the laser because operation close to the cavity stability limit is required [CSM95].

The temporal profile of a pulse generated by a femtosecond oscillator is determined by the Fourier transformation of its spectrum (Eq. (5.6)). If all modes are locked with a constant phase difference between them, the resulting pulse has a minimal pulse duration for the given spectrum. This leads to so-called "bandwidth-limited" or "transform-limited" pulses. For such a pulse the product of the pulse duration and its spectral width (time-bandwidth product) is a constant depending on the pulse shape only. The values of the time-bandwidth products for different commonly used pulse shapes have been given in Sec. 5.1. In the situation when the modes are locked incompletely and the spectral phase depends on the frequency, the pulse duration is longer than the duration of the transform-limited pulse with an identical spectrum. In this case the temporal profile can be derived from the spectrum only if the spectral phase is known.

It is clear that very short pulses can be only generated using broad spectral bandwidth. This bandwidth can be achieved by special crystals doped with a transition metal (titanium, chromium) as gain material [SCB94]. Such materials combine broad fluorescence emission spectra with good thermal conductivity and are very commonly used for the generation of femtosecond pulses. Most important and widely used among them is a sapphire crystal doped with titanium atoms (Ti:sapphire) [Mou86]. It has a gain bandwidth centred around $800\,\mathrm{nm}$. Usually, Ti:sapphire oscillators are pumped by a frequency doubled YAG or argon ion laser [PXK98, MKC99]. Another material is a chromium doped lithium strontium aluminium fluoride (Cr:LiSAF). It generates radiation at the wavelength of $850\,\mathrm{nm}$ and can be pumped by a red diode laser [HVA02]. Finally, chromium doped forsterite (Cr:forsterite) and chromium doped YAG (Cr^{4+}:YAG) lasers operated at $1.2\,\mu\mathrm{m}$ and $1.5\,\mu\mathrm{m}$, respectively, have many applications in the field of microscopy of living systems and metrology [SMB98, AMP05].

5.2.2 Chirped Pulse Amplification

Typical values of the pulse energy delivered by Ti:sapphire femtosecond oscillators lie in the nanojoule range. The task to amplify such pulses to the millijoule level and above is difficult due to the extremely high peak power involved. Stretching the pulse in time by a factor of $10^3 - 10^4$ before amplification solves this problem. There are two ways of the pulse stretching and recompression: prism sequences and grating arrangements [Fre95].

A prism pair can be employed to introduce adjustable GDD and, hence, to stretch or to

recompress a pulse [FMG84]. The angular dispersion of the first prism creates the spatial separation of spectral components of the incoming beam. The second prism is assembled in such a way that the longer wavelength spectral components travel longer distances through the prism material than the shorter spectral components of the beam. This leads to a negative GDD. Recovering of the original beam can be done with either a second pair of prisms or with a reflecting mirror and the same prism pair. In addition, a positive GDD is introduced by the material dispersion when the beam propagates through the prisms. By translation of one prism along its axis of symmetry it is possible to change the thickness of the material transverse by the beam, and therefore achieve a positive GDD. The prism pair allows one to tune the GDD continuously from negative to positive values without beam deviation. Operating the prisms at Brewster angle can minimise the reflection losses for the correctly linearly polarised beam.

A pair of diffraction gratings in a parallel configuration creates a negative GDD in a similar manner as prisms [Tre69]. But the amount of the negative GDD produced by a grating pair can be much larger compared with a prism pair. To minimise the spatial chirp of the output beam parallel alignment of the gratings has to be done with extremely high accuracy. While diffraction gratings are free from material dispersion, optical losses of a grating sequence are quite high even if they are utilised in the Littrow configuration. A pair of diffraction gratings in the antiparallel configuration with a telescope between the gratings is more flexible because of the possibility to introduce both positive and negative GDD [Mar87]. GDD can be controlled by variation of the distance between the second grating and the image of the first grating.

After being stretched, a pulse can be amplified using either a regenerative [WRH94, BKR96] or a multipass [BPH95] amplifier. A regenerative amplifier is a cavity with a gain medium inside. A time gated polarisation devices such as a Pockels cell and a thin film polariser are used to put a pulse into the amplifier. The incoming pulse makes several round trips to gain energy and then it is coupled out of the cavity. Regenerative amplification is the most common technique for the femtosecond pulse amplification because of its reliability, pulse-to-pulse and pointing stability. An alternative and possibly more promising design for femtosecond pulse amplification is based on the multipass scheme. In this configuration an incoming pulse passes through the gain medium several times at slightly different points without using a cavity. Main advantage of the multipass scheme is the ability of generating much shorter pulses than with a regenerative amplifier because this scheme allows one to avoid the large gain narrowing in the

active medium [LSW95]. Moreover, it has a higher gain per pass, and therefore only few passes through the gain medium are required. Thus, the introduced higher order dispersion is rather small and, hence, shorter pulses can be obtained after recompression. Both regenerative and multipass amplifiers are usually pumped either with a frequency doubled, Q-switched Nd:YAG laser at $532\,\text{nm}$ [BGL94] or with an intracavity doubled cw Nd:YLF laser at $527\,\text{nm}$ [BDM97].

The last stage is the pulse recompression. A simplest method involves an identical pair of prisms or gratings as used for pulse stretching. But the amplification process itself leads to extra dispersion, both of second and higher orders. One of the major problem of pulse recompression is to compensate all these contributions. GDD can be totally balanced by a proper compressor alignment. The easiest way to correct the TOD is to adjust the incident angle between stretcher and compressor because of the sensitivity of the third order contribution to this angle [FSR94]. The fact that the third order contribution from a prism pair has the opposite sign compared to a grating pair can be used to compensate the GDD, TOD, and FOD terms as well [FBB87, WRH94]. Another method employs gratings with a different groove density in compressor and stretcher [SBS98]. GDD and TOD can be also corrected by using chirped mirrors [SFS94]. Such mirror consists of multiple dielectric layers with a variable thickness. The penetration depth of the incident radiation depends on its frequency, and therefore reflection from this mirror introduces frequency dependent dispersion. Modern chirped mirrors have a high reflectivity and exhibit dispersion control over a broad spectral range [PKA07].

The pulse duration delivered by CPA systems is mainly limited by two factors. First, the finite bandwidth of the gain medium leads to the spectral narrowing during the pulse amplification and therefore to broadening of the pulse. Second, and more importantly, the higher order dispersion induced in the amplifier results in an additional pulse broadening. A proper compensation of higher order dispersion is a challenging task for laser physics. Many different designs were suggested to overcome this problem [LBa93, WPC93, CRS96, ZMB99]. Up-to-date CPA schemes can provide laser pulses at $1\,\text{kHz}$ repetition rate with up to $15\,\text{mJ}$ energy and a duration below $20\,\text{fs}$ [NKT98].

5.2.3 Multipass Amplification Laser System

A schematic diagram of the multipass amplification laser system utilised in this work is shown in Fig. 5.2. This system consists of the Ti:sapphire oscillator (Femtosource Scientific

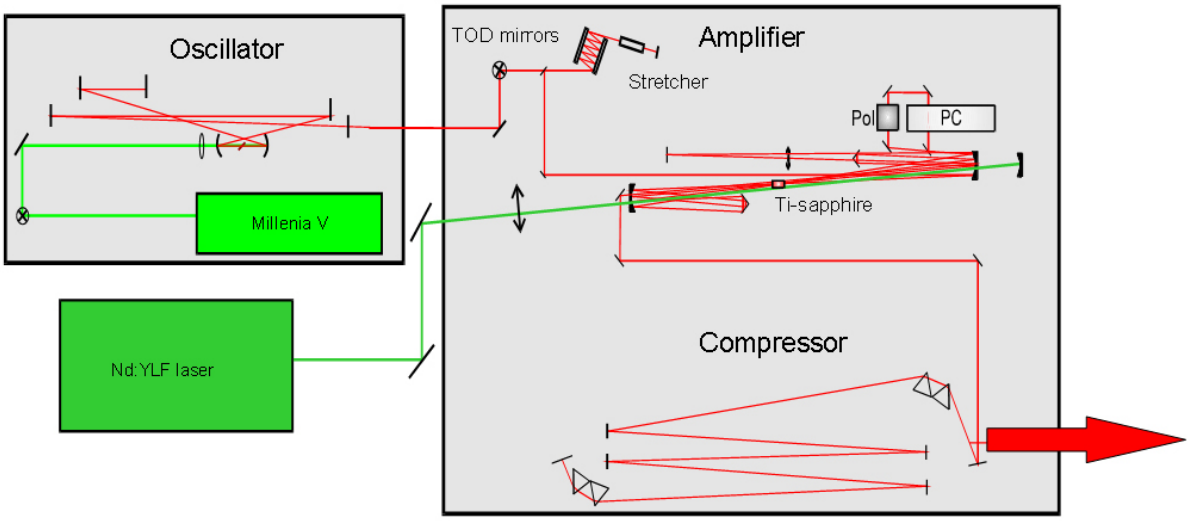

Figure 5.2: Optical layout of the multipass amplification laser system.

PRO, Femtolasers GmbH) pumped by the frequency doubled 5 W Nd:YVO_4 laser (Millennia V , Spectra-Physics Lasers Inc.) and the multipass amplifier (Femtosource Omega PRO, Femtolasers GmbH) pumped by a frequency doubled 13 W Nd:YLF laser (JADE, Thales Laser SA). This system produces laser radiation of 27 fs pulse duration (FWHM) centred at a wavelength of 797 nm with a bandwidth of 45 nm (FWHM) and a repetition rate of 1 kHz. Maximal available pulse energy is 800 μJ. The main parameters of the oscillator and the multipass amplifier are summarised in Table 5.3.

A spatial and directional stabilisation of the output laser beam is implemented using an additional stabilisation system placed behind the amplifier. The stabilisation system is based on the analysis of two beam images created by a pair of CCD cameras which are connected to piezoelectrically controlled mirrors for the motorised correction of the beam position and the propagation direction. This system provides an accuracy of the stabilisation up to $0.5\,\mu$rad [SZH06].

Since the beam diameter after the multipass amplification laser system is larger than the standard size of laboratory optics (1 inch), the laser beam size is decreased by a telescope. It is built by a 2 inch concave mirror with a curvature radius of -2000 mm and a 1 inch convex mirror with a curvature radius of 500 mm. The telescope alignment is done by beam size controlling in the far field. The telescope in the actual configuration reduces the beam diameter four times.

Table 5.3: Output parameters of oscillator and amplifier of the multipass amplification laser system.

Parameters	Oscillator	Amplifier
Central wavelength, nm	~ 785	797
Spectral bandwidth (FWHM), nm	110	45
Pulse duration (FWHM), fs	< 12	27
Pulse repetition rate, Hz	7.5×10^7	1.0×10^3
Pulse energy, μJ	$4 \times 10^{-3} - 6 \times 10^{-3}$	800
Pulse-to-pulse energy stability, % rms	< 0.1	< 1.5

For experiments requiring the second harmonic such as two colour pump-probe or intensity and polarisation dependence studies the second harmonic is generated using a type I of a beta-barium borate (BBO) crystal with a thickness of $50\,\mu$m. The thin crystal has only moderate conversion efficiency for second harmonic generation. The maximal energy of the second harmonic yield is limited to $100\,\mu$J. On the other hand, time the additional dispersion introduced by this thin crystal can be neglected so that a dispersion compensation scheme is not required and the shortest pulses are available directly behind the crystal. The duration of the second harmonic pulses has been measured by a self-diffraction autocorrelator [ZKo02] and is around 25 fs.

5.3 Generation of sub-10 fs Pulses

One of the commonly used and well known techniques for generating sub-10 fs laser pulses is based on spectral broadening in a hollow fiber filled with a noble gas [NSS97, DBK99, SSV04]. The key idea of this technique involves the Kerr type nonlinearity of a noble gas which induces a modulation of the optical phase (Sec. 5.2).

Phase modulation of an optical signal as a consequence of refractive index changes generated by the optical signal itself is called "self phase modulation" (SPM) [KKe95]. SPM leads to a nonlinear shift of frequency components resulting in spectral broadening. The physical

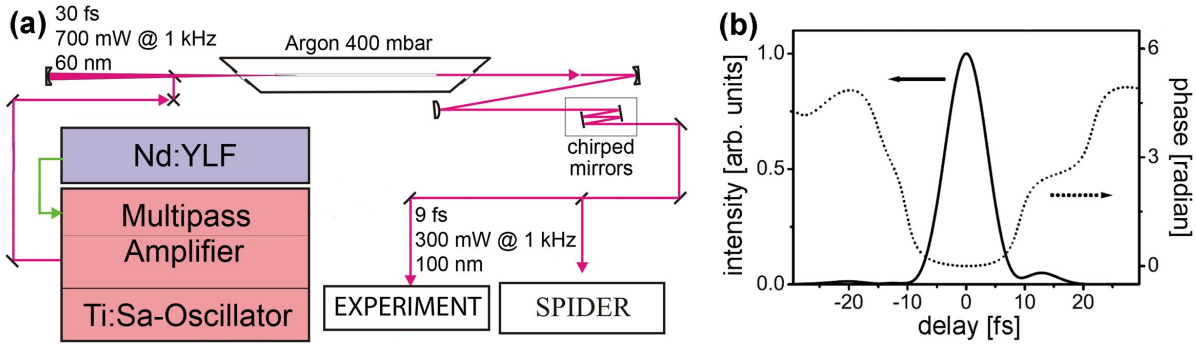

Figure 5.3: (a) Laser setup for the generation of sub-10 fs pulses. (b) Intensity and phase of a pulse with a duration of 8.2 fs measured with the SPIDER technique.

mechanism of this effect is well known [YSh84]. Noble gases exhibit weak nonlinear properties, but long interaction lengths up to 1 m inside the hollow fibre is enough to induce a considerable spectral broadening.

A main inherent restriction of this technique is the rather low output energy due to possible beam distortions and even damage of optical components caused by self-focusing. Typically, hollow fibre compressors deliver laser pulse energies limited to a few hundreds of μJ [KMS00]. Therefore, various alternatives were proposed. To obtain a larger energy with a hollow fibre compressor a so-called "pressure-gradient method" was developed [NSH03]. It provides a better energy transmission through the fibre and was successfully applied for the generation of pulses with a duration of 9 fs at an energy of 5 mJ [SHN05]. Alternatively, fibre free filamentation can be utilised for the generation of sub-10 fs pulses [BKL95, SZS06]. Self-defocusing due to plasma formation in a filament can equilibrate the self-focusing effect from the Kerr nonlinearity. Moreover, this method is less sensitive to experimental parameters such as beam alignment, input pulse duration, or gas pressure [HKH04].

The setup for pulse compression used in this work has been built by the group of Dr. G. Steinmeyer at the MBI and it is depicted in Fig. 5.3a. Laser pulses with a pulse energy of 700 μJ and a duration of 30 fs at 1 kHz repetition rate from a multipass Ti:sapphire amplifier system are focused into a hollow capillary of 48 cm length and 250 μm inner diameter which is filled with 500 mbar of argon to broaden the pulse spectrum. The GDD of the output pulse is then compensated by 4 reflections from specially designed double chirped mirrors that provide a GDD of -60 fs^2 per reflection which leads to the pulse temporal compression. Pulses of up to 300 μJ energy and with a duration down to 10 fs are available after compression [SSt06]. The

temporal profile of compressed pulses is monitored by the SPIDER technique (Sec. 6.1). An example is shown in Fig. 5.3b. The pulse compressor is tuned for the generation of single pulses with suppressed satellites of a shortest possible duration. For example, the pulse presented in Fig. 5.3b has a low satellite content (less than 5% of the pulse peak value) and a duration of 8.2 fs (FWHM) only. All dispersive optical elements between the pulse compressor and the interaction region are doubled in the pulse characterisation arm in order to simulate the real experimental conditions. This allows one to characterise pulses which are identical to those in the interaction region.

5.4 Laser Intensity and Polarisation Control

While carrying out experiments it is often necessary to control and/or change the laser intensity. It is done by the variation of the laser power with two different devises: i) a linear neutral density reflection filter (31W00ML.1, Newport Corp.) or ii) an attenuator consisting of a $\frac{\lambda}{2}$-plate plate coupled with two polarisers (Continuously Variable Attenuator, Altechna Co. Ltd.).

The neutral density reflection filter is a plate with a gradient of a reflectivity across it. The reduction of the laser power is achieved by the reflection of the laser beam from different parts of the plate. The gradient of the reflectivity allows one to reduce the pulse power in the range from 7% to 90%. This reflection method does not introduce any additional dispersion and therefore avoids pulse broadening. It is extremely helpful for the manipulation of sub-10 fs laser pulses. But the neutral density filter has two disadvantages. First, a sharp change of the reflectivity across the plate requires a very precision calibration and reduces the accuracy of the power attenuation. Second, the filter introduces a gradient in the spatial energy distribution of the reflected laser beam.

The second method of the power alteration involves an attenuator which consists of a $\frac{\lambda}{2}$-plate followed by a pair of Brewster type polarisers. The $\frac{\lambda}{2}$-plate rotates the linear polarisation of the incoming laser beam. While the polarisers divide the beam into two orthogonally polarised components. It is preferable to use the reflected vertical polarised part due to the absence of beam transmissions through the polarisers for this component. Two polarisers are utilised to increase a polarisation contrast as well as to keep the output beam parallel to the

input one. The power variation due to the rotation of the $\frac{\lambda}{2}$-plate is

$$P = P_0 \sin^2(2\theta) \quad , \tag{5.31}$$

where P_0 is an input power, P is an output power, and θ is an angle between the horizontal plane and the fast axis of the $\frac{\lambda}{2}$-plate. This method can not be used for the power attenuation of sub-10 fs pulses because the extra dispersion created by the $\frac{\lambda}{2}$-plate. The second limitation is that this attenuator introduces rather large astigmatism.

The polarisation dependent studies on C_{60} require the polarisation variation and control with $\frac{\lambda}{4}$- and $\frac{\lambda}{2}$-plates. A detailed mathematical description of the different optical elements acting on polarised light is given below.

Since light is a transverse electromagnetic wave, the vector of the electric field strength lies in a plane perpendicular to the wave propagation direction. In this plane the electric field vector can be considered as a sum of two orthogonal components in an arbitrary oriented coordinate system. According to [HSc09] Eq. (5.1) for arbitrary light polarisation at the point described by a position vector $\mathbf{r}$ can be presented in a vectorial form as

$$\mathbf{E}(\mathbf{r},t) = \frac{i}{2} A_0 \left[\mathbf{e}\, e^{-i[\omega_0 t - \mathbf{kr} - \phi(\mathbf{r},t)]} - \mathbf{e}^* e^{i[\omega_0 t - \mathbf{kr} - \phi(\mathbf{r},t)]}\right] \quad , \tag{5.32}$$

where $\mathbf{e}$ is an unit polarisation vector and

$$k = \frac{\omega_0}{c} \tag{5.33}$$

is an angular wave number. The polarisation vector can be described in two different basis sets: the Cartesian basis $\mathbf{e}_x$, $\mathbf{e}_y$, $\mathbf{e}_z$ and the spherical basis $\mathbf{e}_{+1}$, $\mathbf{e}_0$, $\mathbf{e}_{-1}$. Assuming propagation of the light along the z-axis (with the x- and y-axes pointed horizontally and vertically, respectively), they are related to each others as

$$\mathbf{e}_{+1} = -\frac{1}{\sqrt{2}}(\mathbf{e}_x + i\mathbf{e}_y) = -\mathbf{e}_{-1}^* \quad , \tag{5.34}$$

$$\mathbf{e}_0 = \mathbf{e}_z \quad , \tag{5.35}$$

and

$$\mathbf{e}_{-1} = \frac{1}{\sqrt{2}}(\mathbf{e}_x - i\mathbf{e}_y) = -\mathbf{e}_{+1}^* \quad . \tag{5.36}$$

According to Eq. (5.32) the linear polarisation along x-axis of the electromagnetic wave is described by

$$\mathbf{E}(\mathbf{r},t) = A_0 \sin[\omega_0 t - \mathbf{kr} - \phi(\mathbf{r},t)]\mathbf{e}_x \quad , \tag{5.37}$$

while the linear polarisation along y-axis leads to

$$\mathbf{E}(\mathbf{r},t) = A_0 \sin\left[\omega_0 t - \mathbf{kr} - \phi(\mathbf{r},t)\right]\mathbf{e}_y \quad . \tag{5.38}$$

Circular polarisation is described by

$$\mathbf{E}(\mathbf{r},t) = -\frac{1}{\sqrt{2}} A_0 \left(\sin\left[\omega_0 t - \mathbf{kr} - \phi(\mathbf{r},t)\right]\mathbf{e}_x - \cos\left[\omega_0 t - \mathbf{kr} - \phi(\mathbf{r},t)\right]\mathbf{e}_y\right) \tag{5.39}$$

and

$$\mathbf{E}(\mathbf{r},t) = -\frac{1}{\sqrt{2}} A_0 \left(\sin\left[\omega_0 t - \mathbf{kr} - \phi(\mathbf{r},t)\right]\mathbf{e}_x + \cos\left[\omega_0 t - \mathbf{kr} - \phi(\mathbf{r},t)\right]\mathbf{e}_y\right) \tag{5.40}$$

for left and right circular polarised light, respectively. In the case of circular polarisation the unit polarisation vector is

$$\mathbf{e}_{el} = e^{-i\delta}\cos\beta\mathbf{e}_{+1} - e^{i\delta}\sin\beta\mathbf{e}_{-1} \quad , \tag{5.41}$$

where β is the so-called ellipticity angle. Combining Eq. (5.32) and Eq. (5.41) one can write the electric field for elliptically polarised light as a column vector

$$\mathbf{E}(\mathbf{r},t) = \frac{1}{\sqrt{2}} A_0 \begin{pmatrix} \sin\beta\sin\left[\omega_0 t - \mathbf{kr} - \phi(\mathbf{r},t) - \delta\right] + \cos\beta\sin\left[\omega_0 t - \mathbf{kr} - \phi(\mathbf{r},t) + \delta\right] \\ \sin\beta\cos\left[\omega_0 t - \mathbf{kr} - \phi(\mathbf{r},t) - \delta\right] - \cos\beta\cos\left[\omega_0 t - \mathbf{kr} - \phi(\mathbf{r},t) + \delta\right] \\ 0 \end{pmatrix} \quad . \tag{5.42}$$

Often, a polarisation ellipse is used to portray the light polarisation. The polarisation ellipse is depicted by a trace of the electric field vector in a plane perpendicular to the direction of the electromagnetic wave propagation. The two semi axes of the ellipse are

$$a = A_0 \sin\left(\beta + \pi/4\right) \tag{5.43}$$

and

$$b = A_0 \cos\left(\beta + \pi/4\right) \quad . \tag{5.44}$$

The ratio of the two semi axes of the ellipse (the ellipticity)

$$\varepsilon = \cot\left(\beta + \pi/4\right) \tag{5.45}$$

together with the angle between the x-axis and the major semi axis (the azimuthal angle) $\phi = \delta$ are an alternative parametrisation of the polarisation state of the light.

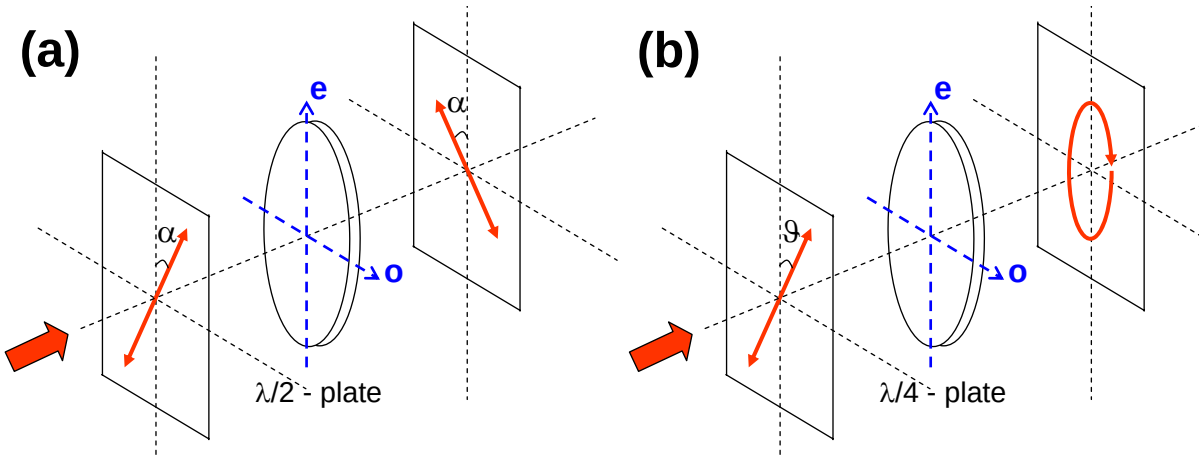

Figure 5.4: (a) The action of the $\lambda/2$-plate on linearly polarised light. The vertical and horizontal dashed blue lines show the extraordinary (optical) and ordinary axes, respectively. Light polarisation (E-vector) is aligned at an angle α with respect to the optical axis of the plate. (b) The action of the $\lambda/4$-plate on linearly polarised light whose polarisation (E-vector) is aligned at an angle ϑ with respect to the optical axis of the plate. For details see text.

$\frac{\lambda}{4}$- and $\frac{\lambda}{2}$-plates are phase retarding devices. They introduce a phase shift Γ between two orthogonally polarised light components (ordinary and extraordinary beams)

$$\Gamma = \omega_0 \frac{d}{c} \left(|n_o - n_e| \right) \quad , \tag{5.46}$$

where d is the thickness of the plate and n_o, n_e are ordinary and extraordinary refractive indexes, respectively. Usually, such plates are produced from a birefringent crystal which is cut so that the extraordinary (optical) axis of the crystal is parallel to the surface of the plate. In particular, $\frac{\lambda}{4}$- and $\frac{\lambda}{2}$-plates create the phase difference of $\frac{\pi}{2}$ and π, respectively. Their action on linearly polarised light is shown in Fig. 5.4.

Linearly polarised light passing through the $\frac{\lambda}{2}$-plate whose polarisation (E-vector) is aligned at an angle α with respect to the optical axis of the plate (as it is depicted in Fig. 5.4a) remains linearly polarised, but the direction of the polarisation is rotated by an angle 2α.

The transmission of linearly polarised light through a $\frac{\lambda}{4}$-plate whose polarisation (E-vector) is aligned at an angle ϑ with respect to the optical axis of the plate is shown in Fig. 5.4b. The result is elliptically polarised light for arbitrary values of ϑ with circular and linear polarisation as limiting cases for some particular values of ϑ. This angle is related to the ellipticity angle β as

$$\beta = \frac{\pi}{4} - \vartheta \quad . \tag{5.47}$$

The alignment of the polarisation ellipse is independent of ϑ. Its principal axes point along the optical axis of the $\frac{\lambda}{4}$-plate and perpendicular to it. Therefore, the ellipse azimuth angle ϕ is 0. If $\vartheta = \pi N$ or $\vartheta = \frac{\pi}{2}(2N+1)$ (N is an integer) the light is linearly polarised along the optical axis or perpendicular to it, respectively. $\vartheta = \frac{\pi}{4}(2N+1)$ corresponds to the circular polarisation.

5.5 Average Intensity of Elliptically Polarised Light

The expression for the instantaneous intensity $I(t,\beta)$ of the elliptically polarised light according to Eq. (5.32) is

$$I(t,\beta) = I_0\left[1 - \sin(2\beta)\left(1 - 2\sin^2(\omega_0 t + \varphi)\right)\right] \quad , \tag{5.48}$$

where I_0 is the laser averaged intensity, ω_0 is the light carrier frequency, and φ is the phase. Eq. (5.48) can be used to describe ellipticity dependence of the ion yield as a function of the laser intensity.

One key difference between linearly and circularly polarised light is the temporal behaviour of its instantaneous intensity $I(t,\beta)$: for linearly polarised light ($\sin(2\beta) = 1$) it varies as $0 \leq I(t,\pi/4) \leq 2I_0$, while for circularly polarised light ($\sin(2\beta) = 0$) it is constant with time $I(t,0) = I_0$.

The excitation probability in a multiphoton process does not directly follow the instantaneous intensity changes with time described by Eq. (5.48) during a single period of the light oscillation. From a classical viewpoint one expects that the overall transition rate in an N-photon process will depend on the time average of the intensity $\langle I^N(t,\beta)\rangle$ which is

$$\langle I^N(t,\beta)\rangle = \frac{\omega_0}{2\pi}\int_0^{2\pi/\omega_0} [I(t,\beta)]^N\, dt \quad . \tag{5.49}$$

Using tabulated expressions for definite integrals Eq. (5.49) can be rewritten as

$$\langle I^N(t,\beta)\rangle = [I_0\cos(2\beta)]^N\, P_N\left(\frac{1}{\cos(2\beta)}\right) \quad , \tag{5.50}$$

where $P_N(x)$ is the Legendre polynomial. Thus, the generalised multiphoton cross-section (see Eq. (3.7)) is expected to depend on the ellipticity angle β. In a direct N-photon process this β-dependent cross-section $\sigma_N(\beta)$ will be largest for linear polarisation ($\beta = \pi/4$) since

the instantaneous intensity variation is largest; and it will become a minimum for circular polarisation ($\beta = 0$ or $\pi/2$), where it is constant with time. For comparison the generalised multiphoton cross-section is normalised to linear polarisation

$$\sigma_N(\beta) = \sigma_N \frac{\langle I^N(t,\beta)\rangle}{\langle I^N(t,\pi/4)\rangle} \quad , \tag{5.51}$$

which replaces σ_N in Eq. (3.7) in a case of elliptically polarised light [SRS09].

In contrast, the time averaged intensity $\langle I(t,\beta)\rangle = I_0$ in a single photon absorption is independent on the polarisation state. Therefore, the excitation probability, which depends linearly on intensity, is independent on polarisation for isotropic targets.

5.6 Pulse Shaping

Femtosecond pulse shaping technique in which practically arbitrary shaped ultrashort laser pulses can be generated is one of the hot topics in modern laser science due to its importance in many areas of physics, material science, chemistry, and biology [JLH07]. Since state of arts in the technique of optical engineering is too slow to directly manipulate an electric field on the femtosecond time scale, pulse shaping can be realised by modulation of the electric field in the frequency domain

$$\tilde{E}_{out}(\omega) = H(\omega)\tilde{E}_{in}(\omega) \quad , \tag{5.52}$$

where $H(\omega)$ is a modulation function, $\tilde{E}_{in}(\omega)$ and $\tilde{E}_{out}(\omega)$ are the spectral representation of the input and output electric field, respectively. The modulation function can modulate spectral amplitude, phase, or polarisation [PWW07]. The resulting temporal structure is determined according to Eq. (5.6) by the inverse Fourier transformation of the modulated spectral representation

$$E^+(t) = \frac{1}{2\pi}\int_{-\infty}^{\infty} \tilde{E}^+_{out}(\omega)e^{i\omega t}\,d\omega = \frac{1}{2\pi}\int_{-\infty}^{\infty} H(\omega)\tilde{E}^+_{in}(\omega)e^{i\omega t}\,d\omega \quad . \tag{5.53}$$

This is the so-called "Fourier transform pulse shaping".

There are three basic techniques of Fourier transform pulse shaping using deformable mirrors [RWW04], acousto-optical modulators (AOM) [DTW97], and liquid crystal modulators (LCM) [WZL01]. A deformable mirror is a membrane mirror driven by a set of electric actuators. The reflective surface of the membrane is displaced by actuators. Therefore, a pulse

shaping with deformable mirrors allows one to make a phase modulation only. Restricted deformations which can be induced on the membrane together with a limited number of actuators constrain the phase variation range. The second technique employs an AOM. Usually, it is a TeO_2 (for the visible light) or InP (for the infrared light) crystal, where modulations of the refractive index are created by the propagation of acoustic waves. Since the transit time of a laser pulse in the crystal is much shorter than the propagation time of an acoustic wave this wave produces a spatial grating which can be considered as a stationary structure on the time scale of the laser pulse propagation through the crystal. The laser pulse diffraction by this structure leads to its spectral modulation. Pulse shaping with an AOM makes available both phase and amplitude modulations. The efficiency of an AOM is limited by $10-15\%$ due to the diffraction nature of this technique. The latter technique is based on a liquid crystal modulator (LCM). An LCM consists of an array of liquid crystal cells (pixels). The refractive index of each pixel can be controlled by applying the voltage across the pixel which generates position dependent either phase or amplitude modulation. The main disadvantage of an LCM is undesirable pulse distortion resulting from the pixellation effects and gaps between the neighbouring cells [Hae04].

Practical implementation of the Fourier transform pulse shaping includes a modulator positioned at the Fourier plane of a $4f$ - zero-dispersion stretcher (compressor) [Mar88]. Basically, the $4f$ - zero-dispersion stretcher consists of a dispersive element (usually a grating) which spectrally separates the input laser beam and a lens or mirror which images the spectrum into the Fourier plane, where the modulator is installed. Subsequently, the second optical arm which is symmetric with respect to the Fourier plane is used to perform the transformation back to the temporal domain. Normal spherical optics are replaced with a cylindrical one that focuses the spectrum in a vertical plane only to avoid a damage of a modulator. The distance between the dispersive elements is equal to four times the focal length of the focusing lens or mirror. In that case the output laser beam has the same characteristic as the input one. If the distance between the focusing elements deviates from $2f$, a temporal dispersion is introduced. Moreover, different spectral components remain spatial distributed across the profile of the the output beam (spatial chirp) if a position of dispersive elements moves aside the focal planes of focusing elements.

Many different schemes for a $4f$ - zero-dispersion stretcher have been suggested [PWA03].

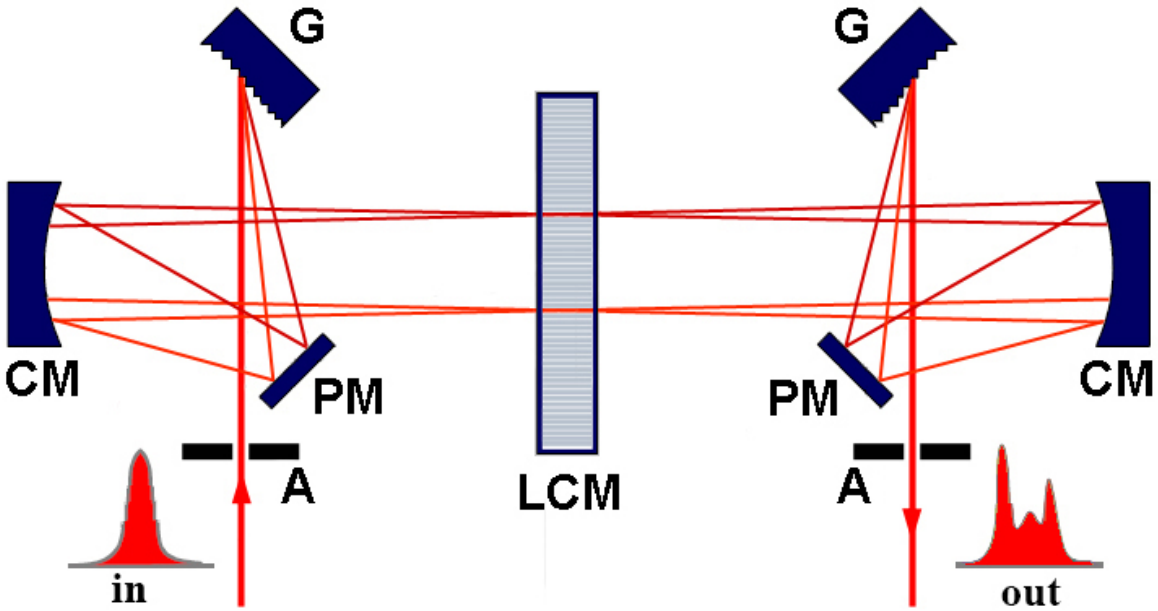

Figure 5.5: Scheme of the pulse shaping setup: A – aperture, G – spectral grating, PM – plain mirror, CM – cylindrical mirror, and LCM – liquid crystal modulator.

The optical layout of $4f$ - zero-dispersion stretcher employed in this work is shown in Fig. 5.5. To minimise beam distortions the laser beam propagates within one horizontal plane only. The input laser beam is diffracted on a spectral grating with $1200\,$lines/mm. The spectrally separated beam is focused after the reflection from a plane mirror by a cylindrical concave mirror with $f = 40\,$cm. An LCM (SLM-S 640/12, Jenoptik GmbH) [SHF01] is placed in a focal plane, where the spectral modulation can be carried out. Next, the optical elements which are symmetric with respect to the position of the LCM reconstruct the output beam. Because lenses introduce chromatic abberations and possess some material dispersion, focusing mirrors are a good alternative for pulse shaping of short laser pulses. The incident angle on the cylindrical mirror has to be as small as possible to minimise astigmatism. All mirrors in this setup have a silver coating. Dielectrically coated mirrors are avoided because of the large phase distortions produced upon a reflection when the incidence angle deviates from a specified value.

Unfortunately, the energy losses of the present pulse shaper setup are rather large. The loss on the diffraction grating even in near the Littrow configuration is $20\,\%$. Each silver coated mirror and the LCM add losses of $7\,\%$ and $15\,\%$, respectively. Hence, the total transmission

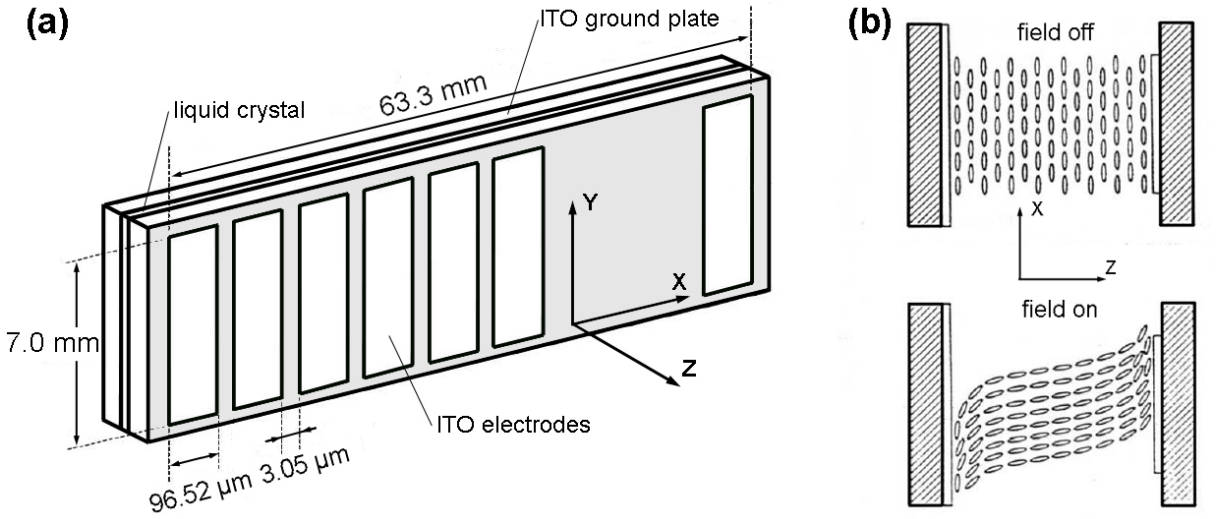

Figure 5.6: (a) The active area of the LCM. (b) Cross-sectional view of the LCM without an electric field applied (top) and with an electric field applied (bottom).

of the pulse shaper setup is around $40\,\%$ only.

The alignment procedure of a $4f$ - zero-dispersion stretcher consisting of multiple optical elements with many degree of freedom is complex. Nevertheless, it is well known and described in the literature [Wei00] and has been used also for aligning the present pulse shaper setup. Directly after the alignment, the duration of the output pulse ($\approx 31\,$fs) is slightly longer than the duration of the input pulse ($\approx 27\,$fs). Temporal profiles of the pulses measured before and after the pulse shaper setup will be reported in Chapter 6 (see Fig. 6.3c and Fig. 6.5c, respectively). A pair of apertures is installed behind and in front of the pulse shaper setup to control the propagation of the laser beam through the setup. Due to the drift of the laser beam periodical adjustment of the propagation direction is required.

The construction of the LCM is shown in Fig. 5.6a. The optical area of the LCM consists of a thin layer ($9\,\mu$m) of a nematic liquid crystal placed between two parallel rubbed glass plates. The plates are coated inside with a indium tin oxide (ITO) which is an electrically conductive but optically transparent material. One coated plate acts as a ground plate, while the coating of the second plate forms an array of 640 electrodes (each $96.52\,\mu$m wide, separated by gaps of $3.05\,\mu$m) that defines the pixels. The active area of the LCM has a height of $7.0\,$mm and a width of $63.7\,$mm. Each pixel can be addressed electronically by applying a voltage between 0 and $8\,$V with a 12-bit resolution (overall 4096 values). The liquid crystal in the gaps can not be controlled.

The parallel rubbing of the glass plates causes an orientation of long rod-like molecules of the liquid crystal along the rubbing direction (x-axis in Fig. 5.6). This substrate possesses optical anisotropy and acts as a birefringent uniaxial crystal with its optical axis parallel to the molecular orientation. For light propagating in z-direction the refractive index in the xz-plane (extraordinary refractive index n_e) differs from the refractive index in the yz-plane (ordinary refractive index n_o). When the voltage is applied between the electrodes, the molecules of the liquid crystal have a tendency to be oriented in the direction of the applied electric field (z-direction) and the extraordinary refractive index is changed. Thus, the applied voltage controls the birefringence and modifies the optical path length which induces a phase delay (retardation)

$$\Gamma(U,\lambda) = \frac{2\pi d}{\lambda}\left(n_\theta(U,\lambda) - n_o(\lambda)\right) \quad , \tag{5.54}$$

where $n_\theta(U,\lambda)$ is the voltage dependent extraordinary refractive index ($n_\theta(0,\lambda) \equiv n_e(\lambda)$), d is the thickness of the liquid crystal layer, U is the applied voltage, and λ is the wavelength of the light passed through the liquid crystal layer. The dependence of the extraordinary refractive index on the applied voltage is

$$\frac{1}{n_\theta^2(U,\lambda)} = \frac{\cos^2\left(\theta(U)\right)}{n_e^2(\lambda)} + \frac{\sin^2\left(\theta(U)\right)}{n_o^2(\lambda)} \quad , \tag{5.55}$$

where $\theta(U)$ is an angle of the liquid crystal molecules tilt induced by the applied voltage [Jen02]. This angle increases monotonous as a function of the applied voltage.

The calibration of the LCM requires knowledge about the phase retardation. It can be determined from the measurement of a light transmission $T(U,\lambda_{ref})$ at some wavelength λ_{ref} with crossed polarisers [Hen03]. The LCM inside the $4f$ - zero-dispersion stretcher is placed between two crossed polarisers in xy-plane oriented at $+45\,^\circ$ and $-45\,^\circ$ with respect to x-axis (see Fig. 5.6) and transmission at λ_{ref} as a function of the driver voltage value can be measured by a spectrometer. This transmission depends on the phase retardation according to [Jen02] as

$$T(U,\lambda_{ref}) = \sin^2\left(\frac{\Gamma(U,\lambda_{ref})}{2}\right) \quad . \tag{5.56}$$

The transmission curve measured at $\lambda_{ref} = 800\,\text{nm}$ and utilised for the LCM calibration is shown in Fig. 5.7a. By measuring transmission at different wavelengths information about the wavelengths λ propagating across each pixel of the LCM P_N can be obtained. This dependence

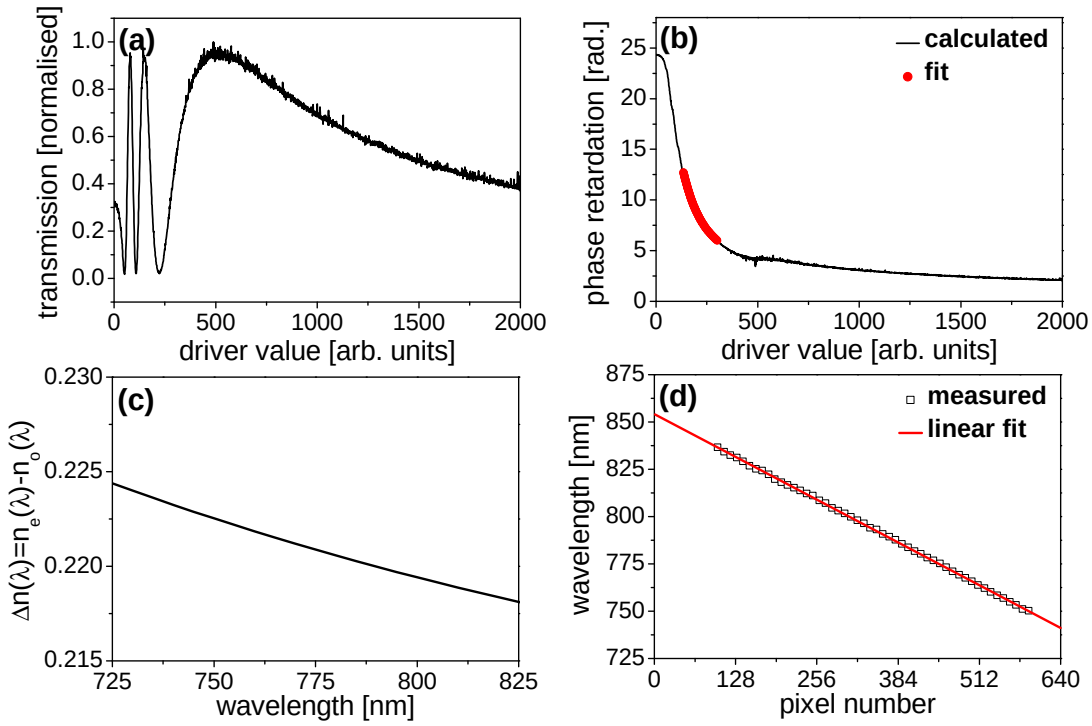

Figure 5.7: Calibration of LCM: (a) measured transmission function $T(U, \lambda_{ref})$ ($\lambda_{ref} = 800\,nm$); (b) recalculated phase retardation $\Gamma(U, \lambda_{ref})$ and its fit; (c) wavelength dependence of the dispersion $\Delta n(\lambda)$; (d) wavelength dependence on the pixel number of the LCM.

depicted in Fig. 5.7d is clearly linear

$$\lambda = -0.17644 P_N + 854.10441 \quad , \tag{5.57}$$

while coefficients (-0.17644 and 854.10441) are determined by the alignment of the $4f$ - zero-dispersion stretcher and a position of the LCM. The phase retardation recalculated from Eq. (5.56) as

$$\Gamma(U, \lambda_{ref}) = \arcsin\left(\sqrt{T(U, \lambda_{ref})}\right) \pm 2\pi k \tag{5.58}$$

is presented in Fig. 5.7b. The phase retardation $\Gamma(U, \lambda)$ at an arbitrary wavelength can be converted to the retardation $\Gamma(U, \lambda_{ref})$ at the known wavelength as

$$\Gamma(U, \lambda_{ref}) = \Gamma(U, \lambda) \frac{\lambda}{\lambda_{ref}} \frac{\Delta n(\lambda_{ref})}{\Delta n(\lambda)} \quad , \tag{5.59}$$

where $\Delta n(\lambda) = n_e(\lambda) - n_o(\lambda)$. $\Delta n(\lambda)$ is approximated by the following expression

$$\Delta n(\lambda) = \lambda \sqrt{\frac{0.04008}{\lambda^2 - 0.10722}} \quad , \tag{5.60}$$

where λ is measured in μm [Jen02]. This dependence is shown in Fig. 5.7c. The recalculated phase retardation $\Gamma(U, \lambda_{ref})$ together with Eq. (5.59) and Eq. (5.60) can be used for the LCM calibration.

A voltage needed to obtain the required phase retardation at some arbitrary pixel of the LCM can be calculated using the following procedure. First, the wavelength λ corresponding to this pixel has to be determined using Eq. (5.57). Second, the required phase retardation at this wavelength has to be converted to the known retardation at the wavelength λ_{ref} according to Eq. (5.59) and Eq. (5.60). Third, the driver voltage value can be calculated using the following expression

$$U = -71.6 + 1483.5 \exp\left(-\frac{\Gamma(U, \lambda_{ref})}{2.1}\right) + 389.0 \exp\left(-\frac{\Gamma(U, \lambda_{ref})}{19.7}\right) \quad . \tag{5.61}$$

This expression is derived from a fit of the known data $\Gamma(U, \lambda_{ref})$ and presented in Fig. 5.7b. In spite of the LCM capability to retard the phase up to approximately 5π at $800\,\text{nm}$, the maximal phase retardation is restricted by 2π during the calibration procedure. Possible values of the phase retardation lies in the range between 2π and 4π.